Numerical Investigation of Cold-Formed Purlins with Longitudinal Stiffeners in Shear

A Thesis

Submitted in Partial Fulfilment of the Requirements

For the Degree of

Master of Engineering

In

Structural Engineering

By

Yosep Caceres Callo

SID 490179419

Supervisor: Cao Hung Pham

School of Civil Engineering

University of Sydney, NSW 2006

Australia

June 2020

DISCLAIMERS

Student Disclaimer

The work comprising this thesis is substantially my own, and to the extent that any part of this work is not my own I have indicated that it is not my own by acknowledging the source of that part or those parts of the work. I have read and understood the University of Sydney Student Plagiarism: Coursework Policy and Procedure. I understand that failure to comply with the University of Sydney Student Plagiarism: Coursework Policy and Procedure can lead to the University commencing proceedings against me for potential student misconduct under chapter 8 of the University of Sydney By-Law 1999 (as amended).

Departmental Disclaimer

This thesis was prepared for the School of Civil Engineering at the University of Sydney, Australia, and describes experiments to induce breakage in a calcareous sand by compression and shearing. The opinions, conclusions and recommendations presented herein are those of the author and do not necessarily reflect those of the University of Sydney or any of the sponsoring parties to this project.

ABSTRACT

In the steel building industry, Cold-formed steel (CFS) members have a variety of applications, being purlins one of particular interest, these structural members are usually used to transfer roof desk loads to the structural frames. CFS enables to manufacture of purlins in different complex shapes, and one of them are channels with longitudinal web stiffeners. It is known that the addition of longitudinal web stiffeners increases the shear strength capacity of CFS channels; however, it is not evident in how much. In that sense, this thesis presents a numerical investigation on shear buckling and shear strength of CFS purlins with inclined longitudinal web stiffeners.

This research involves the development of a numerical model of the novel Dual Actuator Test Rig, which enables the shear study of CFS purlins with high aspect ratio (shear span/web depth). This stage of the investigation is based on the Finite Element Method (FEM) by using the software ABAQUS/Standard. Afterwards, FEM-ABAQUS simulations have been performed on channels with inclined longitudinal web stiffeners and aspect ratio of 2.0. More precisely, five stiffened web channels with different stiffener depths and a constant width of 5.0 mm were simulated along with an additional reference unstiffened channel.

The relationship between the inputs, inclined longitudinal web stiffeners and initial geometric imperfections, and the outputs, failure mode, shear buckling and shear strength, were deeply discussed to understand better the shear behaviour of the stiffened web channels and its correlation with the unstiffened channel. Furthermore, the FEM outcomes were subsequently plotted against Direct Strength Method (DSM) shear curves, to verify the accuracy of the numerical results and the reliability of the current DSM shear equations.

ACKNOWLEDGEMENTS

I want to thank my supervisor, Doctor Cao Hung Pham for his guidance and support throughout the present research. I would also like to thanks Ph.D. candidate Duy Khanh Pham for his guidance in the used of ABAQUS modelling.

I want to express my eternal gratitude to my parents for their love, wisdom and support. I am also grateful to my siblings for their continuous encouragement. Similarly, I would like to thank my partner in love Roxana for her unconditional love and support, and my beloved daughter Killary for her understanding throughout this study period far away from home.

I am genuinely thankful to the Peruvian Government, specifically to PRONABEC program for granted scholarship, without their financial and economic support this journey would never be possible.

Table of Contents

List of Figures

List of tables

ABBREVIATIONS

CFS: Cold-formed Steel

DSM: Direct Strength Method

EWM: Effective Width Method

FEM: Finite Element Method

HRS: Hot-rolled Steel

SFSM: Spline Finite Strip Method

SAFSM: Semi-Analytical Finite Strip Method

TFA: Tension Field Action

1. INTRODUCTION

1.1. Background

Worldwide, there are two principal types of structural steel, and they are Cold-formed steel (CFS) shapes and Hot-rolled steel (HRS) shapes. The manufacturing process of CFS differs from HRS in the required temperature to be formed, requiring low and elevated temperatures, respectively. Additionally, the slender properties of CFS members, with a thickness range from 0.4 mm to 6.4 mm, make possible manufacture a great variety of shapes that with HRS are not viable.

CFS members in building construction began to be used around the 1850s in the United States and Great Britain. However, they were not wildly used until 1946 when the American Iron and Steel Institute (AISI) included specifications for its design. Since then, CFS member uses and applications has grown continuously. [1] Moreover, CFS structures are very popular around the globe; basically because of its excellent strength-to-weight ratio, ease assemble and economical transportation and handling. Besides, it represents a sustainable building alternative due to its recyclable material properties. [2]

In the building industry, there is a variety of applications for CFS sections, being the principals framing, metal buildings and racks. However, the current improvement not only in the analysis but also in the design of CFS members makes this versatile material advance from being used in low-rise buildings to mid-rise buildings. Likewise, computational software and tools allow the industry to manufacture complex and optimized shapes that successfully would meet the new structural requirements. [3]

Among the variety of applications of CFS members; purlins are one of particular interest. Commonly used in roof systems, this structural member is in charge to transfer loads from the roof decks to the main structural frames. Furthermore, CFS purlins are usually made from high strength steel, reaching yield stresses up to 550 MPa. This high strength results in a reduction of thickness, which in turn allows manufacturing a variety of complex shapes. The production of CFS purlins involves a cold-forming process, in which flat sheet steel is bent at ambient temperature.

In the Australian and New Zealand market, novel and innovative CFS purlins have been incorporated over the last 20 years. There are three types of CFS purlins, being commonly utilised the plain sections C and Z, which include lips in both flanges, as shown in Fig.1.1 (a); then it is the Supa sections C and Z, which include lips and small longitudinal web stiffeners as shown in

Fig.1.1 (b). Finally it is the DHS section, which includes longitudinal intermediate web stiffeners, as shown in Fig.1.1 (c). As we can appreciate in Fig. 1.1, the development consist of the inclusion of additional flange, web or lip stiffeners in the section in order to increase its strength capacity. [4]

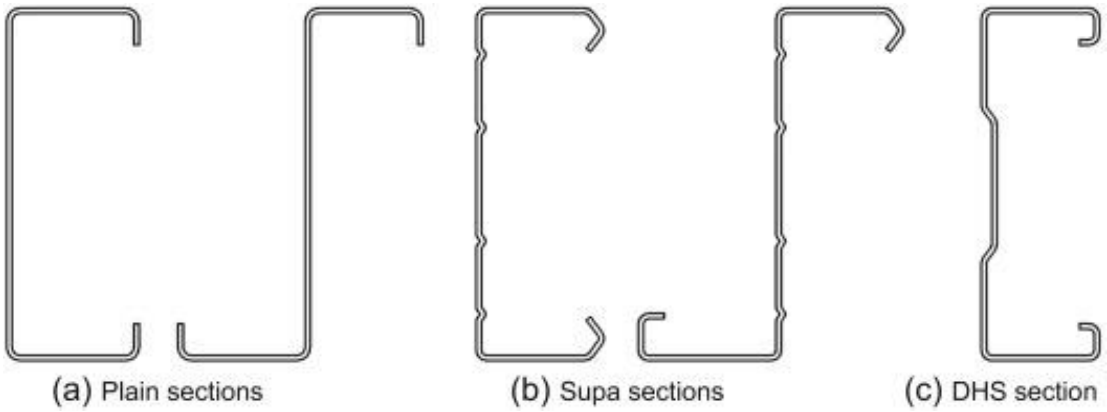

Figure 1.1 Profile shapes of manufactured purlins [4]

Currently, the estimation of shear capacity for purlins with longitudinal intermediate web stiffeners is a matter of ongoing investigations. No standard in the world contains equations for directly calculate both shear buckling and ultimate shear strength. Furthermore, the strength capacity of this CFS purlins is believed to be underestimated since the equations are semi-empirical and have been calibrated against experimental test with a significant presence of bending moment and shear aspect ratio of 1.0.

1.2. Statement of Problem

Experimental and Numerical investigations for shear aspect ratio of 1.0 have proven that longitudinal web stiffeners improve the shear strength of CFS purlins. Even though the shear span was short enough to minimise the effect of bending moment, the influence of this remaining bending on the shear strength capacity could have been underestimated. Therefore, there is a need for understanding the shear behaviour of longitudinally stiffened web purlins with high shear aspect ratio at least possible bending.

1.3. Scope and objectives of the research

The research aims to provide an understanding of the mechanical behaviour of CFS purlins with longitudinal stiffeners and higher span ratio predominantly in shear. Numerical investigation is performed followed by an analysis and discussion of results using the Direct Strength Method (DSM) curve for CFS sections in shear. In order to achieve these objectives, the following tasks are addressed:

- Conduct numerical simulations based on the Finite Element Method (FEM) to validate the Test Rig numerical model of a plain cold-formed C-lipped section subjected to predominantly shear.
- Perform a series of nonlinear numerical simulations for CFS purlins with longitudinal stiffeners and aspect ratio of 2.0 to broaden the knowledge about their shear behaviour.
- Study the shear strength and elastic buckling of stiffened web CFS purlins with different sizes predominantly in shear.
- Compare the numerical test results with the current DSM curves for shear design of CFS members.

1.4. Research Methodology

The approach is to perform a numerical investigation based on the validation of one experimental specimen results collected using the novel Dual Actuator Test Rig. In that sense, the software package ABAQUS/CAE is employed to perform a series of nonlinear finite element simulations for purlins with longitudinal stiffeners. These simulations are then calibrated to satisfy the bending moment condition of the Test Rig to finally determine the Ultimate Shear Strength (V_T) of the sections. Afterwards, these previous ABAQUS models are employed for performing the shear elastic buckling analyses and get; as a result, the shear buckling loads (V_T) for sections with different longitudinal web stiffeners. Finally, both results, shear ultimate strength and shear elastic buckling, are collected for their comparison with the DSM design loads for shear.

2. LITERATURE REVIEW

2.1. Design criteria of CFS purlins

The slender thickness and the cold-forming process of CFS purlins set a group of failure modes that are a matter of concern for the design phase. As structural thin-walled elements, CFS purlins are subjected to load conditions like bending moment, axial and shear forces. The combination of these loads can provoke different failure issues, which are known as buckling. Thus, the buckling analysis is crucial for a proper design. Furthermore, axial and bending stress can trigger a range of buckling failures, such as flexural, flexural-torsional, distortional or local buckling. Currently, all of them are well understood; therefore, Hancock [5] first proposed a curve that describes the buckling stresses versus half-wavelength of a buckle. This curve is commonly known as "signature curve", and a particular example is shown in Fig. 2.1 [4].

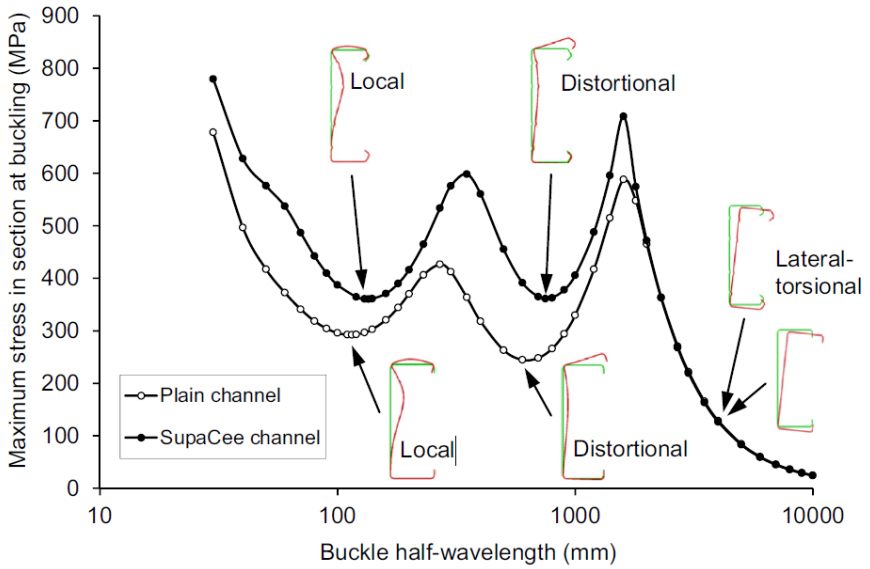

Figure 2.1 Flexural signature curve and buckling modes of cold-formed plain C-sections and SupaCee sections. [4]

On the other hand, the typical approach to analysing the shear stress was focused on the web without considering any other component in the analysis. Consequently, only shear local buckling was obtained under pure shear loading. Nevertheless, new analytical and numerical methods allow studying the shear stress of the whole section. This fact makes possible the manifestation of distortional shear buckling in the analysis. Therefore, purlins under pure shear can cause buckling of the whole section in the form of either local or distortional buckling. Thus, it is necessary to differentiate each of them since that is the main issue in this investigation.

2.2. Elastic Shear Buckling of thin structures

When it comes to analysing slender rectangular plates in shear, the governed failure mode is commonly shear buckling. The shear buckling stress was formulated by Timoshenko and Gere [6] as follows:

$$\tau_{cr} = \frac{k_v \pi^2 E}{12(1-\mu^2)}\left(\frac{t}{h}\right)^2$$

Where E is Young's modulus, μ is the Poisson's ratio, h is the depth of the plate, t is the thickness of the plate element, and k_v is the shear buckling coefficient, which depends on the boundary conditions and the aspect ratio, $\alpha = a/h$, in which a represents the length of the plate element. The following equations can determine the value of k_v for simple supported edges:

$$k_v = 4.00 + \frac{5.34}{\alpha^2}, when\ \alpha \leq 1$$

$$k_v = 5.34 + \frac{4.00}{\alpha^2}, when\ \alpha > 1$$

However, CFS sections are usually conformed by webs, flanges and lips, which makes the previous approach obsolete to analyse the shear buckling of the full section; because only analyse the behaviour of the web ignoring the rest components. Pham and Hancock [7] adapted the Spline Finite Strip Method (SFSM) to a computational program in order to study and analyse the shear buckling behaviour of the whole section. For that purpose, C-sections of various lengths with and without lips were analysed under four different shear flow distributions, as shown in Fig. 2.2. The results show that the flanges and lips can significantly improve the shear buckling capacity of the thin-walled section. Furthermore, it was also demonstrated that a broad enough flange prevents premature torsional and lateral buckling.

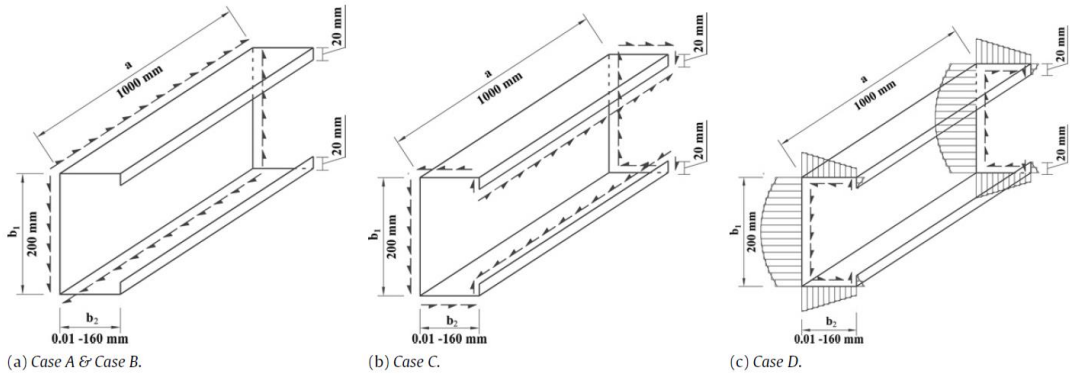

Figure 2.2 Shear flow distribution in lipped sections. [7]

Hancock and Pham [8] investigated the shear buckling modes using the Semi-Analytical Finite Strip Method (SAFSM) and reproduced the signature curve for a channel section under shear.

Fig. 2.3 shows the signature curve for the buckling stress versus the buckle half-wavelength for a single half-wavelength. Where usually, the local buckling dominates at short half-wavelengths, and distortional buckling is evident at longer half-wavelength in some cases. Additionally, to implement the method, a computer program called bfinst7.cpp, written in Visual C++, was successfully developed and used for the investigation.

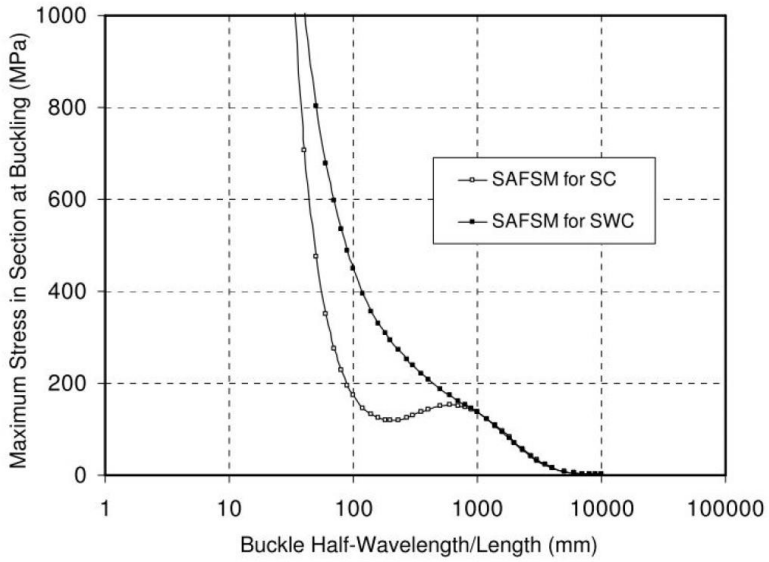

Figure 2.3 SAFSM Signature Curves of Plain Lipped Channel (SC) and Stiffened Web Channel (SWC) [8]

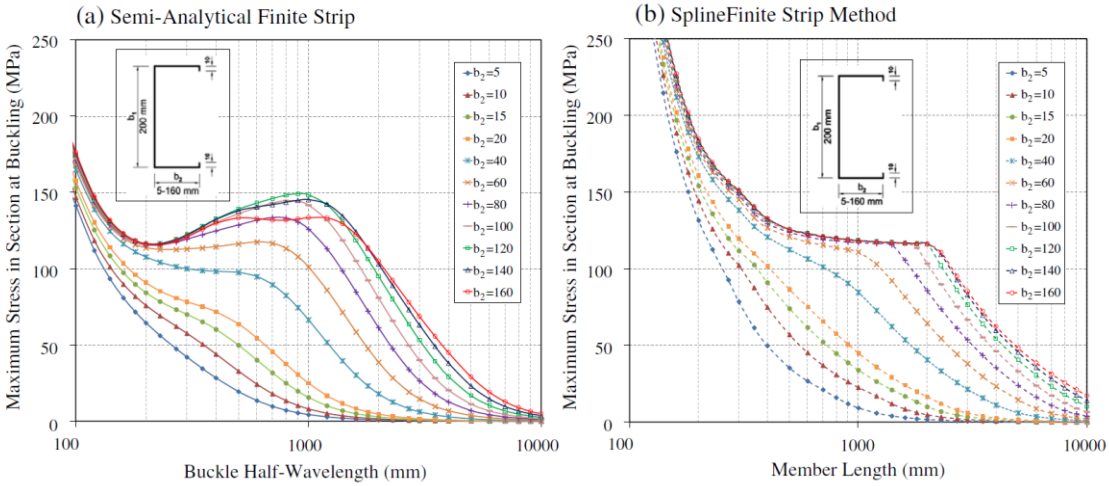

Figure 2.4 Shear buckling stress vs buckling half-wavelength/length of unlipped channel sections.[9]

Similarly, Pham and Hancock [9] analysed channel sections subjected to pure shear stresses using the SAFSM and the SFSM. Both differ from each other in the type of used function for the longitudinal direction; SAFSM employs harmonic series, whereas SFSM uses local spline functions. Likewise, they have different boundary conditions; SAFSM is free to distort in its two-section ends; in contrast, SFSM is simply supported at its all end edges. Therefore, SFSM can include multiple

buckling modes, whereas SAFSM is limited to a single half-wavelength. The analysis results show that the shear buckling stress decreases dramatically as the length of the section increase. Moreover, as shown in Fig. 2.4, while longer is the length, more similar are shear buckling values of both approaches; however, for short lengths, they differ significantly due to the different boundary conditions. Additionally, the flange width determines at what length the buckling mode switches from local to distortional buckling.

Later, Hancock and Pham [10] enhanced their previous developed SAFSM method to allow the simply supported boundary condition and combined loading. This novel method, recall as reSAFSM (restrained SAFSM) has been successfully derived and programmed in Visual Studio C++, giving as a result bfinst8.cpp programme. This new computer programme was used to verify the accuracy of the method, which in general is in significant agreement with the SFSM. Furthermore, its powerful graphical function allows a 3D plot of the shear buckling modes, as shown in Fig. 2.5.

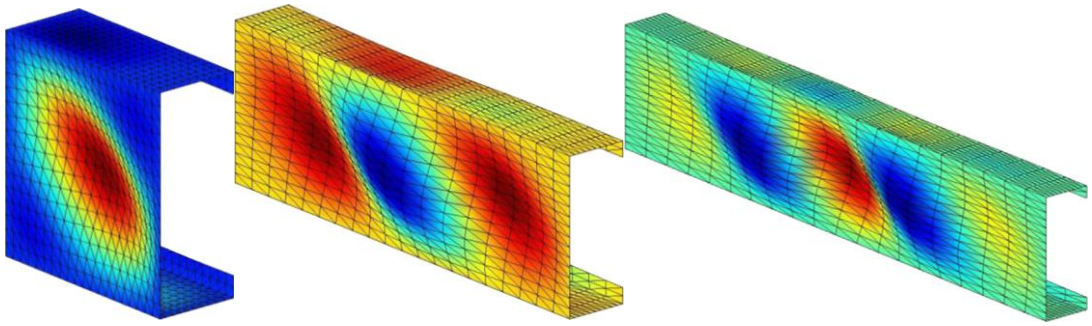

Figure 2.5 Shear buckling mode of a simple lipped channel
at lengths of 200, 600 and 1000 mm. [10]

2.3. Codes and Standards

In worldwide design specifications, there are currently two methods to verify the strength and serviceability of CFS members. These are the Effective Width Method (EWM) and the Direct Strength Method (DSM). Between these two methods of design, DSM appears to be more practical and accurate; especially when it comes to analysing complex sections in which the computation of effective width becomes challenging. Nowadays, it is most common to find complex CFS sections on the market; and the estimation of the effective width of various components turns out to be complicated for EWM. Not to mention that in some cases, there is not a design approach using EWM. It is in that context that DSM approach becomes more relevant and gets ahead of EWM, since better performs the structural behaviour of CFS section; which is achieved by analysing the buckling stresses of CFS sections as a whole rather than by parts as EWM does. Hence, in an attempt to design everyday most complex CFS sections, DSM represents a more straightforward and more accurate approach.

2.3.1 Direct Strength Method of Cold-formed Steel Members

The Direct Strength Method (DSM) of cold-formed steel structural members is formally available in design specifications around the world. Being the most relevant, the North American Specification for the design of cold-formed steel structural members AISI S100:2016 [11] and the Australian-New Zealand Standard for cold-formed steel structures AS/NZS 4600:2018 [12]. Both standards are very similar, and they have been crossed-referenced to each other. However, what tell them apart is the characteristics of materials, loading conditions and types of infrastructures that are independent of each nation. That said, when it regards to research investigation AISI S100:2016 is more cited, for that reason we will refer to this standard for the present investigation.

The reliability of DSM for compression and bending has been well investigated. Likewise, it has been extended for pure shear and combined shear and bending. Even though the method has been proved to be accurate, it requires the computation of shear buckling, for which numerical shear buckling analysis is performed. Moreover, the shear strength is predicted by DSM, with a semi-empirical approach which is a matter of several ongoing investigations. That is why the design rules of DSM for shear will be reviewed hereunder.

2.3.2 DSM Design Rules for Members in Shear

2.3.2.1 DSM Design Rules in Shear without Tension Field Action

The nominal shear strength (V_n) of beams without holes in the wed and without transverse web stiffeners is determined from Section G2.1 of AISI S100-16 [11] as follows:

$$\text{For } \lambda_v \leq 0.815,\ V_n = V_y \tag{1}$$

$$\text{For } 0.815 \leq \lambda_v \leq 1.227,\ V_n = 0.815\sqrt{V_{cr}V_y} \tag{2}$$

$$\text{For } \lambda_v > 1.227,\ V_n = V_{cr} \tag{3}$$

$$V_y = 0.6A_wF_y \tag{4}$$

$$V_{cr} = \frac{k_v\pi^2 E A_w}{12(1-\mu^2)\left(\frac{h}{t}\right)^2} \tag{5}$$

where A_w is the area of the web element, F_y is the design yield stress, V_y is the yield shear force of cross-section, μ is the Poisson's ratio, V_{cr} is the elastic shear buckling force of the whole section, $\lambda_v = \sqrt{V_y/V_{cr}}$, k_v is the shear buckling coefficient of the whole section.

2.3.2.2 DSM Design Rules in Shear with Tension Field Action

For members without holes in the wed and with transverse web stiffeners, the nominal shear strength (V_n) of beams is determined from Section G2.2 of AISI S100-16 [11] as follows:

For $\lambda_v \leq 0.776$, $V_n = V_y$ (6)

For $\lambda_v > 0.776$, $V_n = \left[1 - 0.15\left(\frac{V_{cr}}{V_y}\right)^{0.4}\right]\left(\frac{V_{cr}}{V_y}\right)^{0.4} V_y$ (7)

2.4. Experimental and numerical study

2.4.1 Experimental investigation of CFS members with longitudinal web stiffeners in shear

Pham, Bruneau and Hancock [13] employed a test rig apparatus, which previously was used by Pham and Hancock [14], to investigate the shear behaviour of longitudinal web stiffened cold-formed purlins with an aspect ratio of 1.0 as shown in Fig. 2.6. This test was similar to the one developed by Yu and LaBoube [15], except for the fact that they used five rows of bolts distributed along with the full depth of the section instead of four as it was first proposed. Allowing the modified test, the development of full tension field action and consequently an increment on the shear strength on the studied specimens. One of the main conclusions in the investigation of Pham, Bruneau and Hancock [13] was that the effect of the residual bending moment on the shear strength was more pronounced in the longitudinally web stiffened purlins than in the flat ones. Consequently, the interaction between bending and shear is more significant for longitudinally stiffened web purlins.

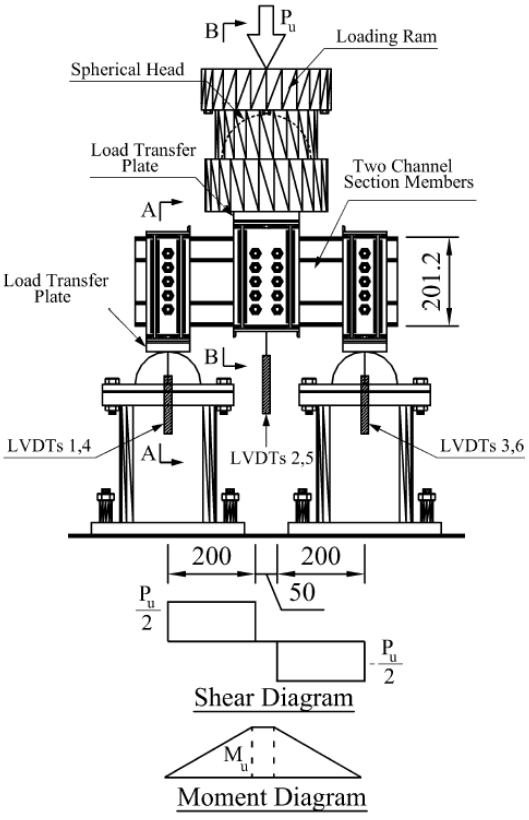

a) Testing apparatus

b) Shear failure mode of a purlin with longitudinal web stiffener and aspect ratio of 1.0, SWC-R90 × 15.

c) Shear failure mode of a purlin with longitudinal web stiffener and aspect ratio of 1.0, SWC-R20 × 15.

Figure 2.6 Test configuration by Pham, Bruneau and Hancock [13]

Afterwards, in an attempt to minimise and manage the influence of bending moment in pure shear tests, in the J.W. Roderick Laboratory for Materials and Structures at the University of Sydney, a new test rig has been developed for solving this issue. This equipment, known as the dual actuator rig, allows testing specimens primarily under shear loads with minimal bending moments for span ratios equal to or higher than 1.0 [16]. Fig. 2.7 shows a schematic diagram and a 3D rendered image of the dual actuator test configuration. Pham, Pham and Hancock [16] have performed an experimental program in plain C and SupaCee® cold-formed steel sections by using the dual actuator rig. Being the main remark that the dual actuator rig is proven to be accurate and reliable to experimentally study the shear strength of CFS members with aspect ratios of 1.0 or higher.

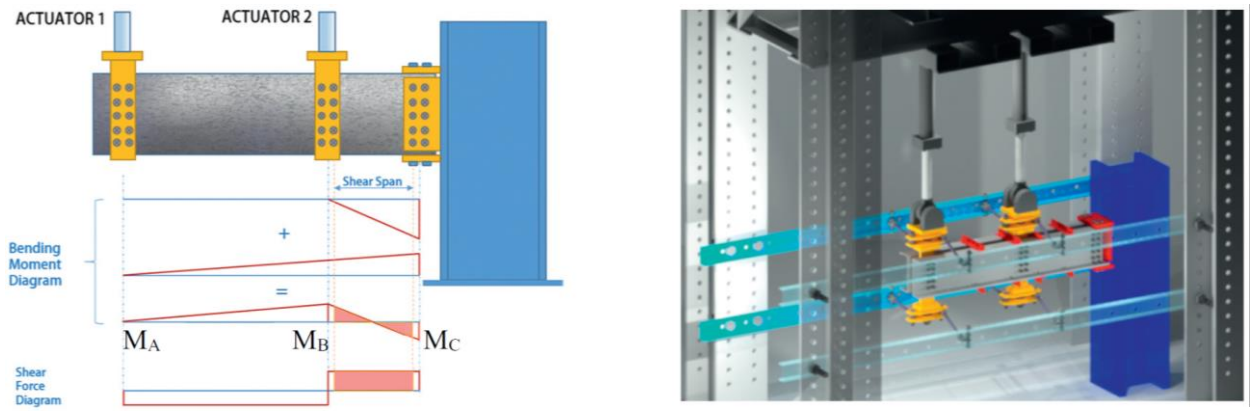

a) Bending and shear diagrams of the test. b) 3D rendered image of the test setup

Figure 2.7 Dual actuator configuration [16]

2.4.2 Numerical Investigation of CFS members with longitudinal web stiffeners in Shear

Pham, Pham and Hancock [17] performed a numerical study of the elastic shear buckling of CFS members with three different types of web stiffeners under pure shear. The study proved that the presence of longitudinal web stiffeners improves the elastic shear buckling stress of sections. Besides, it was demonstrated that the whole web buckles locally when the stiffeners are very small. Fig. 2.8 shows the buckling analysis of rectangular stiffeners where b_{s1} represents the depth of the stiffener for a stiffener width $b_{s2}$of 15 mm.

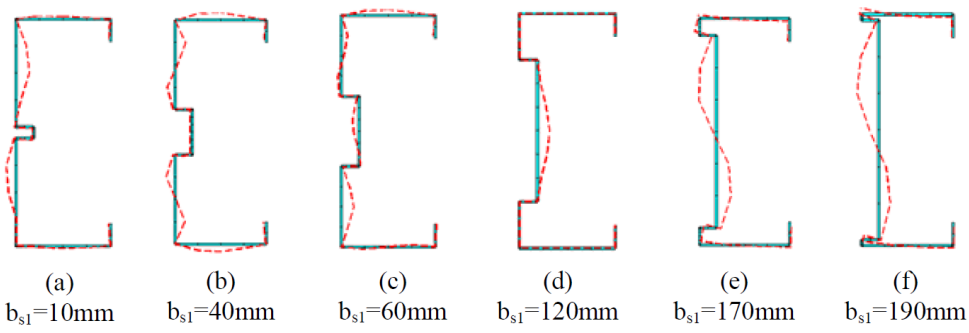

Figure 2.8 In-plane buckling analysis of members with rectangular web stiffeners [17]

Later, based on an experimental study presented in [13], Pham and Hancock [18] performed a finite element simulation of CFS members with longitudinal rectangular web stiffeners. Using the software package ABAQUS/Standard, the numerical investigation predominantly in shear showed a good agreement with the experimental results, allowing the usage of the model to extend the data range.

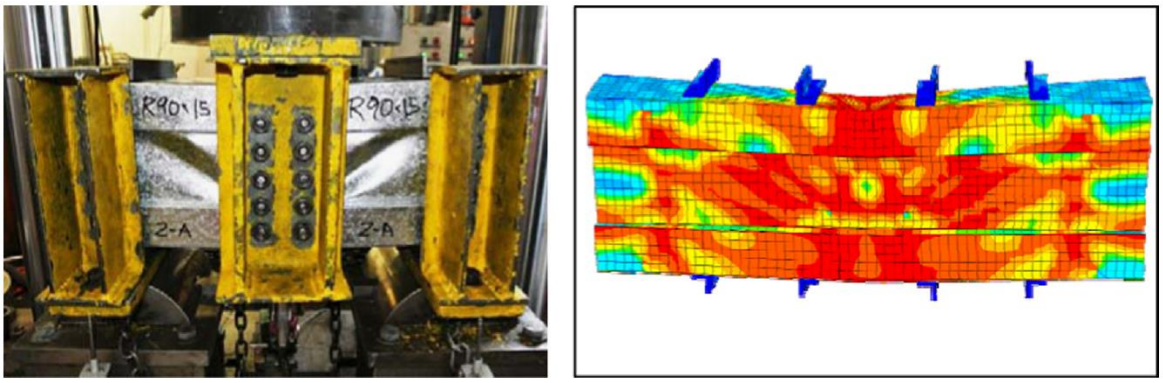

Figure 2.9 Experimental test and numerical ABAQUS model SCW20012-R90x15 [18]

2.4.3 Dual Actuator Test configuration and instrumentation

The configuration of the test is that two vertical forces are applied to a cantilever CFS beam. The idea behind the test rig is to generate a pair of bending moments with the same magnitude but with opposite direction at the two ends of the shear span matter of interest. Consequently, the moment to shear ratio for this test rig is half of the conventional point central test, which is beneficial for studying the pure shear condition.

Furthermore, the test specimen is bolted to 20 mm thick plates on the web and the flanges, which in turn are welded to a rigid column. The two actuators transfer vertical loads to the specimen through 20 mm thick loading plates, which are bolted to the CFS purlins web using five rows of M12 high strength bolts as shown on Fig. 2.10. Both MTS actuator has a capacity of 253 kN and 162 kN, in compression and tension respectively, and has a stroke of 508 mm. The actuators are controlled simultaneously by an MTS FlexTest® Controller. They can move independently at different speeds; which could be adjusted as convenient. Hence, the end moments of the shear span could be managed and controlled throughout the experiment keeping the ratio of -1.0 between them. [16]

For tracking the deformation and displacements of the specimens, ten linear variable displacement transducers (LVDTs) are used throughout the test. All of them are arranged in the following manner, two LVDTs are employed to track the horizontal displacement of the column which has a rigid connection with the beam specimen, and six LVDTs are used to measure the vertical movement along the length of the beam. The remaining two are allocated in the diagonal centre of the shear panel to track the out of plane deformation. [16]

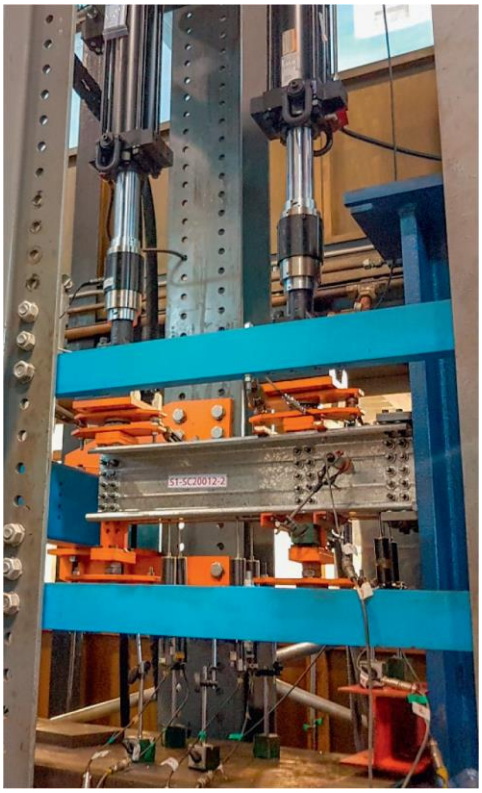

a) Overall view

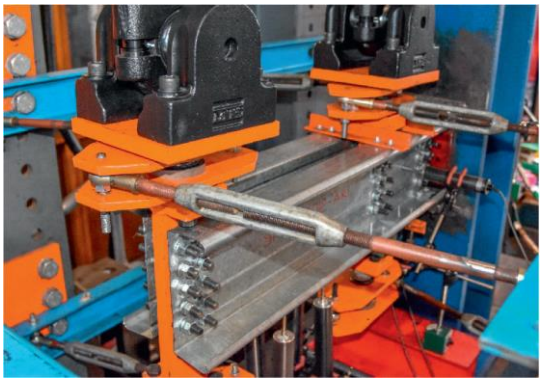

b) Side view

c) Front view

Figure 2.10 General test configuration of the dual actuator [16]

3. NUMERICAL INVESTIGATIONS

3.1. General

This chapter describes a series of nonlinear numerical simulations, using the software package ABAQUS/Standard based on the finite element method (FEM), on high strength CFS sections with longitudinal purlins subjected to predominantly shear. For validating the simulations of this purely numerical investigation, the experimental test results of plain C-channel with shear aspect ratio of 2.0, perform by Pham, S.H. [19] were used to compare and calibrate its conducted numerical simulation. Thus, ensure the accuracy before being utilised to conduct parametric studies and examine the shear behaviour of various longitudinally stiffened web purlins in greater detail.

3.2. Model details

In ABAQUS/Standard, two different element types were adopted to model the Dual Actuator Test Rig simulation. In that sense, 4-node doubly curved shell elements (S4R), which has been successfully used by diverse researchers, were selected to model cold-formed steel purlins. Likewise, 8-node linear brick elements (C3D8R) were used to model the rest components, which include the angle straps, plates and the column. In both cases, reduced integration and hourglass control option were selected for modelling.

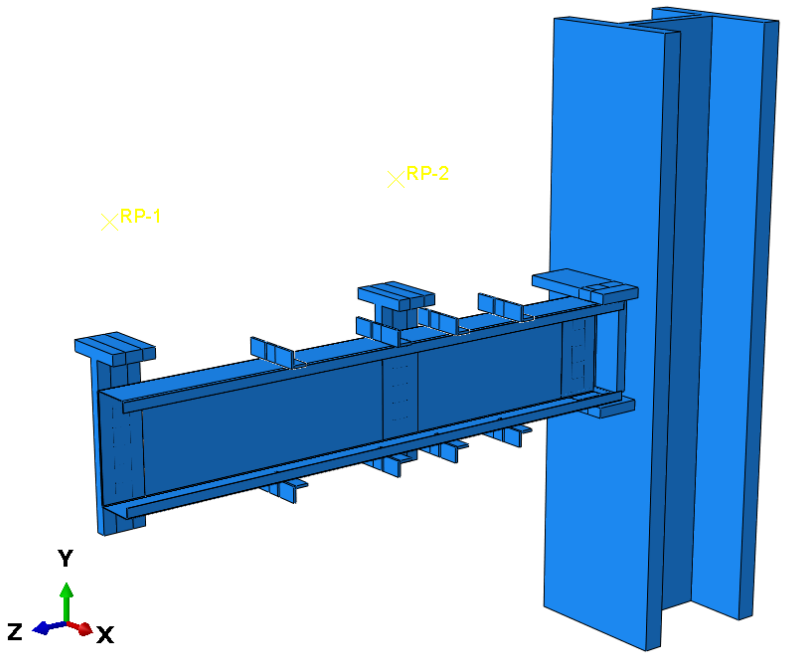

Figure 3.1 Three-dimensional view of the FE model

The numerical configuration of the Test Rig is similar to the one developed by Pham, S.H. [19], as seen in Fig. 3.1. Unlike the actual test, only one channel was modelled due to the symmetry condition of having two channels bolted to two sides of the loading plates, and the angle straps were modelled imposing X-symmetry boundary conditions on their back end. Moreover, the vertical displacements generated by the two actuators were resembled by applying displacement boundary conditions on the top of the loading plates. Likewise, discrete fastener elements were used to simulate the M12 bolts that connect the channel web to the loading plates and M10 bolts that connect the channel flanges to the top and bottom plates, respectively. Attachment lines were allocated at the location of the bolts, and subsequently, connector sections were assigned to them. Additionally, these connectors have been assigned with nonlinear elastic behaviour and generic "cartesian + rotation" properties.

Furthermore, an ENCASTRE boundary condition was imposed at the column base to prevent all the degrees of freedom and simulate its fixed condition. In order to model the welded connections between the three plates and the column a tie constraint was employed to restrain translational or rotational movement of the plates. Lastly, the interaction between the purlin channel and the different plates were resembled by imposing surface to surface contact.

3.3. Material properties

To perform the nonlinear analysis in ABAQUS/Standard, both the true stress (σ_{true}) and the true plastic strain (ε_{true}) are required as input for the stress-strain data. This data is generated from the engineering stress and strain of coupon test, and has to be processed as follows:

$$\sigma_{true} = \sigma(1 + \varepsilon)$$

$$\varepsilon_{true} = \ln(1 + \varepsilon) - \frac{\sigma_{true}}{E}$$

where

σ is the engineering stress,

ε is the engineering strain,

E is Young's modulus.

In general, two different material types were defined in all the simulations, one for Cold-Formed Steel (CFS) and another for Hot-Rolled Steel (HRS). Moreover, the material properties of both CFS and HRS were taken from the tests performed by Pham S.H. [19]. In that sense, the input elastic properties of CFS are as follows: an average Young's modulus of

200951 MPa, mean yield stress of 584.2 MPa and a typical Poisson's ratio of 0.3. Meanwhile, the true stress-strain data, derived from the coupon tests shown in Fig. 3.2, was defined for the nonlinear plastic analysis. Fig. 3.3 illustrates the true plastic stress-strain curve of 1.2 mm thick CFS channel.

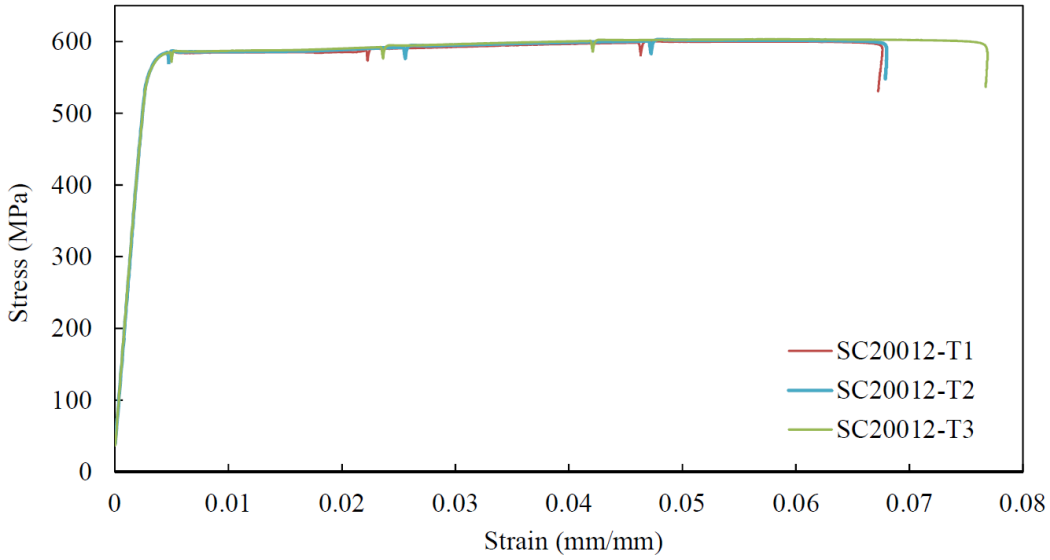

Figure 3.2 Coupon test results of 1.2 mm thick plate [16]

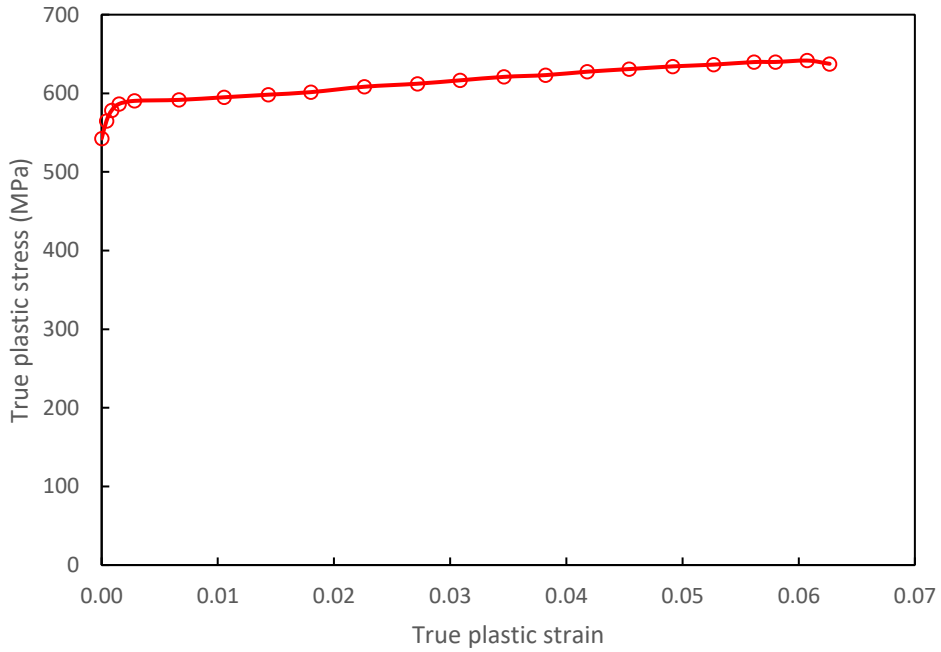

Figure 3.3 True plastic stress-strain curve of 1.2 mm CFS channel

Furthermore, the elastic material properties of HRS are the following: Young's modulus of 200000 MPa and Poisson's ratio of 0.3, while the true stress-strain curve, shown in Fig.3.4, was used as input to define the plastic behaviour of HRS members.

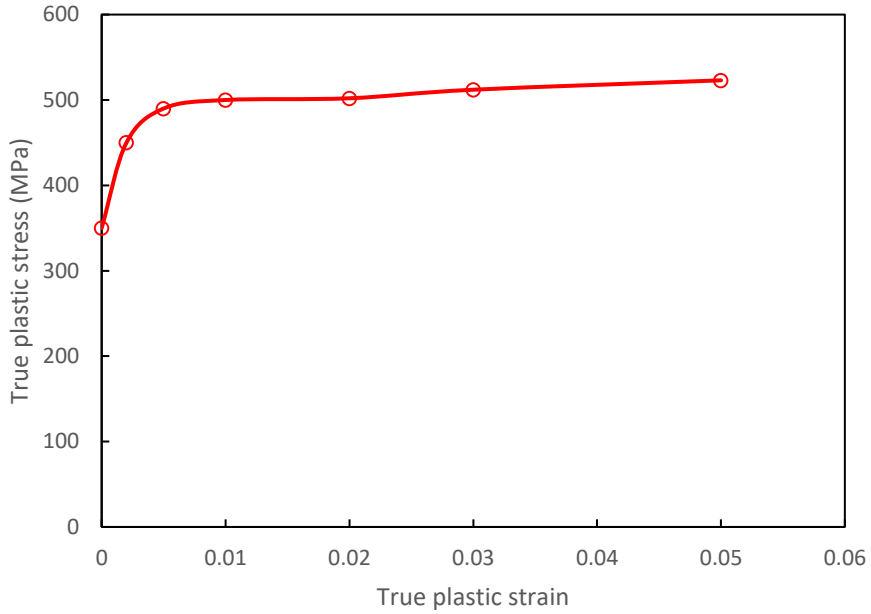

Figure 3.4 True plastic stress-strain curve of HRS members

3.4. Solution control

In order to analyse both the buckling and post-buckling response, two different analyses were carried out throughout the numerical investigation in ABAQUS/Standard. For buckling response, the eigenvalue buckling analysis was performed by defining the Buckle step via linear perturbation procedure and using subspace eigensolver in order to obtain the shear buckling load. Meanwhile, the Riks method was employed for the post-buckling response. This approach is capable of solving a post-buckling problem for either stable or unstable response. Additionally, it has been proven to be accurate and reliable when analysing the shear strength of CFS members.

3.5. Mesh convergence study

It is essential to point out that the principal member of the numerical model is the channel section; consequently its mesh size is decisive for the numerical investigation. In order to find an optimal mesh size, a mesh convergence study has been developed to determine the mesh size that guarantees the accuracy of results and efficiency of computational time. Hence, Fig. 3.5 shows an interaction line between the number of mesh elements and the peak shear strength carried for a single test channel. It can be seen that the higher the number of mesh elements, the better the convergence of the shear strength. Furthermore, six different mesh sizes were plotted on the graph, and it was observed that the mesh size of 5x5 mm is reasonable enough to get accurate results efficiently. Regarding the other

members of the simulation, a 10x10 mm mesh size has been proposed for all of them.

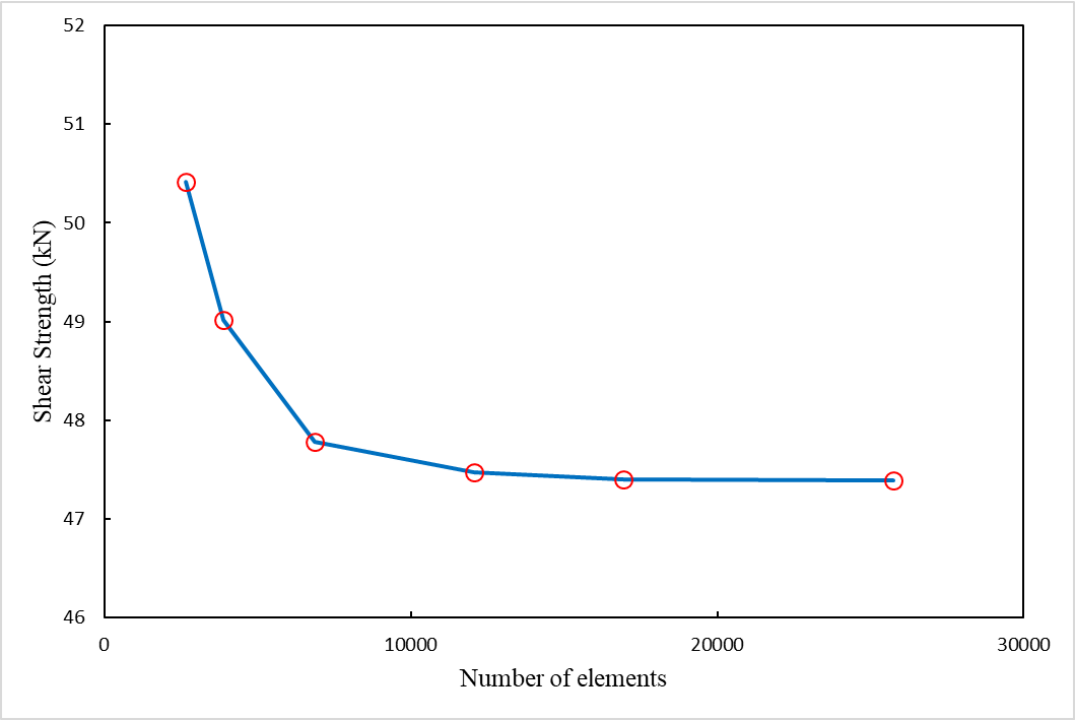

Figure 3.5 Mesh convergence study

3.6. Validation of FE models

In order to validate the numerical investigation, one specific model was replicated to verify its accuracy with respect to the experimental test developed by Pham S.H. [19]. In that sense, the shear buckling load and shear strength of one specific simulation will be compared with the real experimental results. The purpose of this numerical investigation is to analyse CFS purlins with higher aspect ratio. Therefore the chosen specimen corresponds to a Plain Cee section with a shear span of 400 mm, and an aspect ratio of 2.0, further the thickness of the member is 1.5 mm. Table 3.1 summarises the dimensions and material properties, while Table 3.2 shows the experimental result of CFS member. The information provided in Tables 3.1 and 3.2 were gathered from the Pham S.H. research investigation.

Table 3.1 Dimensions and material properties [16]

Test	t (mm)	D (mm)	B (mm)	L (mm)	f_y (MPa)	E (MPa)
C20015-2	1.54	204.50	75.60	16.30	538.9	205157
	1.54	204.00	75.20	16.70		
Mean	1.54	204.25	75.40	16.50	-	-

Table 3.2 Experimental results [16]

Test designation	Section Type	Shear span (mm)	Aspect ratio	Vn, test (kN)
C20015-2	Plain Cee	400	2	47.50

3.6.1. Validation of buckling analysis

For guaranteeing the reliability of the buckling analysis, the results were compared with the outcomes obtained by Pham S.H. [19]. Thus, BFINST8 [16], a computer program based on the Semi-Analytical Finite Strip Method (SAFSM), was used on mentioned research to validate the buckling behaviour. Table 3.3 compares the buckling load of the selected C20015 section obtained by Pham S.H and the proposed FEM Abaqus model. It was found that the developed numerical model has more variance than the one developed by Pham S.H. In fact, there is a 4.4% difference with respect to the BFINST8 model.

Table 3.3 Buckling loads comparison

Section	Shear span (mm)	Aspect ratio	Vcr (kN) Pham S.H.			Vcr (kN)	
			SAFSM (BFINSTS)	FEM (ABAQUS)	Variance (%)	FEM (ABAQUS)	Variance (%)
C20015	400	2	24.3	24.9	2.47	25.36	4.36

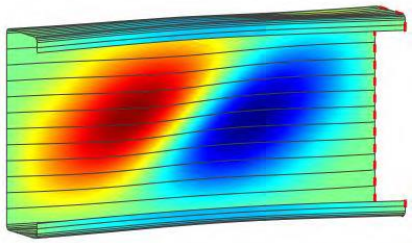

a) Buckling mode shape (SAFSM)

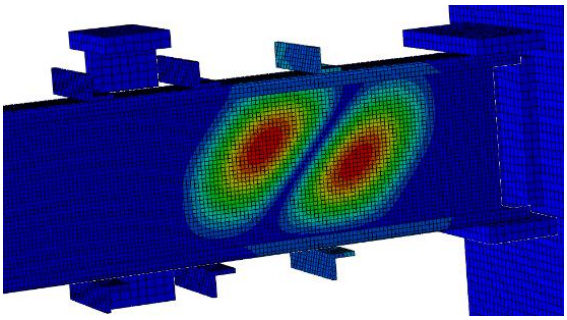

b) Buckling mode shape (FEM Abaqus)

Figure 3.6 Buckling mode shape of section C20015 with shear span 400 mm

Moreover, Fig. 3.5 compares the buckling mode shapes of the section under study produced by the SAFSM and by the proposed FEM simulation. In both cases, two shear buckle occurred and are very similar. Hence, the good agreement between SAFSM and FEM simulation exhibit that the proposed FEM models are capturing well the buckling behaviour of the member.

3.6.2. Validation of ultimate strength analysis

In order to validate the FEM developed model, the strength analysis outcomes were compared with experimental strength results. To be specific, the peak shear force and failure mode of the numerical and experimental outcomes were contrasted with each other. The mean geometric dimensions and plastic properties of the test specimen were input for the numerical simulation. Furthermore, using the linear superposition of buckling eigenmodes, initial imperfections were incorporated into the simulation. The escalating factors of 0.15t and 0.64t, being t the thickness of the CFS member, were imposed into the model to account for initial geometric imperfections. These two values have been used on previous numerical studies by Pham and Hancock [18] and Pham S.H. [19]. After the model was build and analysed, its shear strength outcomes were compared with experimental test results, as shown in Table 3.4. The shear strength obtained from simulations with and without initial imperfections is close to each other. Besides, the model with an imperfection factor of 0.64t has a variance of 2.7%.

Table 3.4 Initial imperfection

		V_{FEM} (kN)				
Section	Aspect ratio	0t	0.15t	0.64t	V_{Test} (kN)	Variance (%)
C20015	2	47.55	47.21	46.21	47.50	-2.72

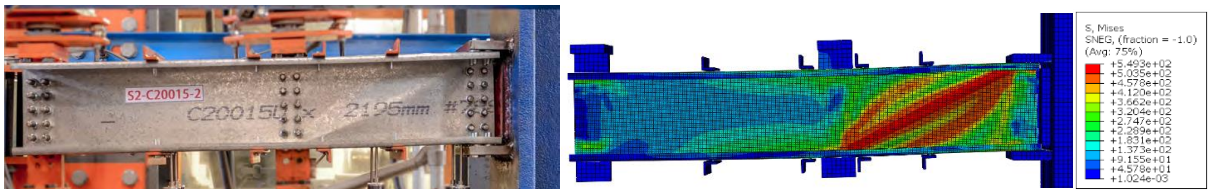

a) Experimental test [19] b) FEM model

Figure 3.7 Failure mode comparison between test and FEM simulation

Fig. 3.7 compares the shear failure mode produce by the experiment and by the FEM simulation. Further, the Von mises stress distribution of the FEM simulation is shown in Fig. 3.7 (b). Moreover, it can be seen that the FEM model resembles well the failure mode of the experimental test.

Therefore, the numerical simulation of the test rig Dual actuator can be used for further studies, which include the numerical investigation proposed on the present research, analyse the influence of including longitudinal stiffeners on the member web.

3.7. Parametric study of purlins with different longitudinal stiffeners size

For the parametric analysis, the material properties and geometric dimensions of the CFS member were modified; however, the rest elements of the Dual Actuator simulation were kept without any modification. The nonlinear material properties are already defined in Section 3.3 while the geometrical properties and a description of various CFS sections are defined in the following lines.

In order to perform the numerical investigation, six different simulations were build based on a plain lipped C-channel of 200 mm with flange and lip dimensions of 80 mm and 20 mm respectively. Then five different stiffened web channels were simulated with one longitudinal web stiffener but with different sizes. The geometrical dimensions of the five longitudinally stiffened web channels and plain lipped C-channel are shown in Table 3.5, where D is the web depth, B is the flange width and L is the lip size, being all of them outside dimensions. Additionally, b_{s1} is the stiffener width while d_{s1} and d_{s2} are the inner and outer depths of the inclined stiffener. The stiffened web channels have an indent of 5 mm and two segments inclined 45º; these portions join the inner and outer web sections. Further, they all have a thickness of 1.2 mm and a corner radius of 2.0 mm. The six types of cross-sections used for the numerical study are shown in Fig. 3.7.

Table 3.5 Geometric dimensions of the specimens

Section label	t (mm)	D (mm)	B (mm)	L (mm)	b_{s1} (mm)	d_{s1}(mm)	d_{s2} (mm)
C20012	1.2	200.0	80.0	20.0	-	-	-
SWC-I-20-5	1.2	200.0	80.0	20.0	5.0	20.0	30.0
SWC-I-40-5	1.2	200.0	80.0	20.0	5.0	40.0	40.0
SWC-I-60-5	1.2	200.0	80.0	20.0	5.0	60.0	70.0
SWC-I-80-5	1.2	200.0	80.0	20.0	5.0	80.0	90.0
SWC-I-100-5	1.2	200.0	80.0	20.0	5.0	100.0	110.0

C=plain lipped C section, 200 outer section depth and 12 thickness times 10 in mm
SWC=Stiffened web channel, I=Inclined stiffener and "20-5" inner depth and width of the stiffener respectively

The nonlinear analysis of the seven sections was performed by adding initial geometric imperfections into the perfect FEM models, and, as in section 3.5.2, the imperfection scaling factors of 0.15t and 0.64t were introduced to predict the ultimate shear loads on the six specimens. Table 3.6 summaries the ABAQUS-FEM results of the eighteen predominantly shear test for proposed sections of study. Overall, it can be seen that the models' results with

and without geometric imperfections are very close to each other. Further, the models with 0.64t imperfections highly influence on reducing the ultimate shear strength, and it is more notorious for sections with larger stiffeners width, more precisely sections SWC-I-80-5 and SWC-I-100-5, with a variation of 10.6% and 12.1%, respectively. In previous FEM studies performed by Pham and Hancock [18] and Pham S.H [19] the simulations with 0.64t geometric imperfection give closest results to the experimental test, so based on that fact, the shear strength forces with this imperfection will be assumed as the ultimate shear strength loads of the member.

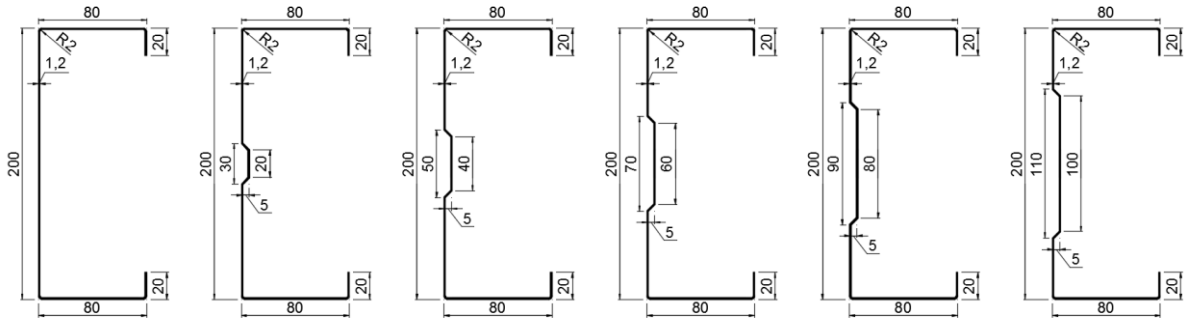

Figure 3.8 Section types used for the numerical study

Table 3.6 ABAQUS-FEM results of shear strength

Section	Aspect ratio	Shear span (mm)	V_{FEM} (kN)			Variation (%)
			0t	0.15t	0.64t	
C20012	2.0.	400	36.80	34.83	34.78	5.49
SWC-I-20-5	2.0	400	39.51	39.44	39.11	1.01
SWC-I-40-5	2.0	400	43.18	43.12	43.07	0.25
SWC-I-60-5	2.0	400	43.02	42.91	41.71	3.05
SWC-I-80-5	2.0	400	42.21	38.44	37.75	10.58
SWC-I-100-5	2.0	400	41.15	36.10	36.19	12.05

Fig. 3.8 shows the failure mode of the six numerical specimens with their respective Von Mises stress distribution at the peak shear load with their respective colour scale chart. All the presented outcomes correspond to the simulations with 0.64t geometric imperfection. It can be seen that unlike from expected the failure mode of some simulations is not in predominantly shear. Four out of the six simulations fail in pure shear, as seen in Fig. 3.8 (a), (b) (d) and (f). The failure mode of the remaining two is unclear, as appreciated in Fig. 3.8 (c) and (d), for some reason, they could not reach the shear failure mode. Moreover, the bending moment values at the failure mode are also important to guarantee a shear failure mode. As summaries,

in Table 3.7, the ratio between moment and shear is around 0.20, which is excellent in the attempt to reduce the influence of bending on the shear tests and especially for large aspect ratio.

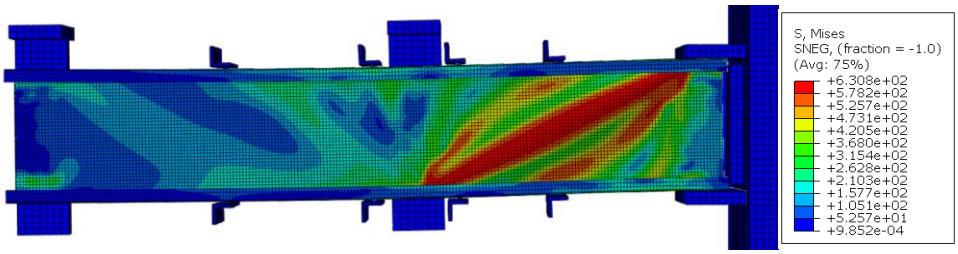

(a) Section C20012

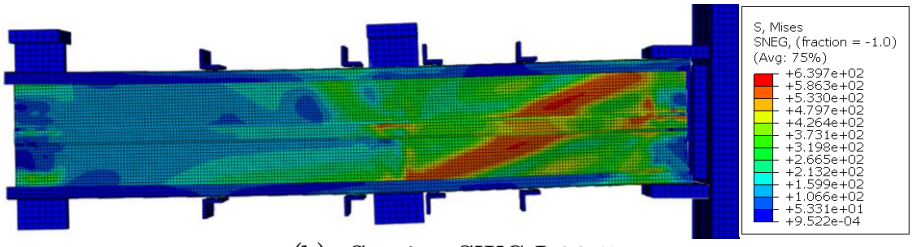

(b) Section SWC-I-20-5

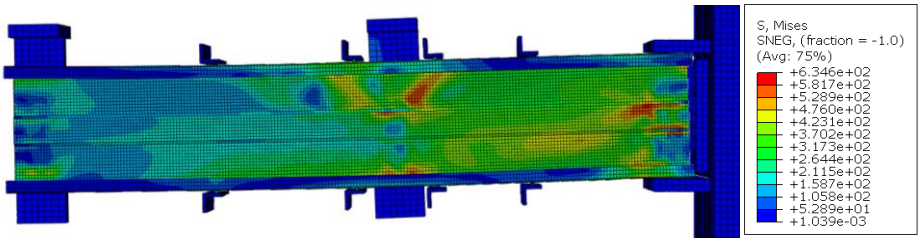

(c) Section SWC-I-40-5

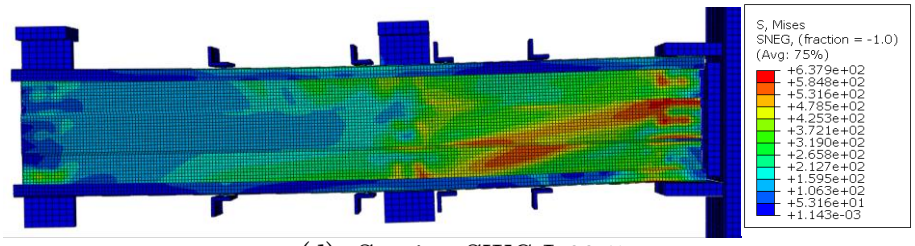

(d) Section SWC-I-60-5

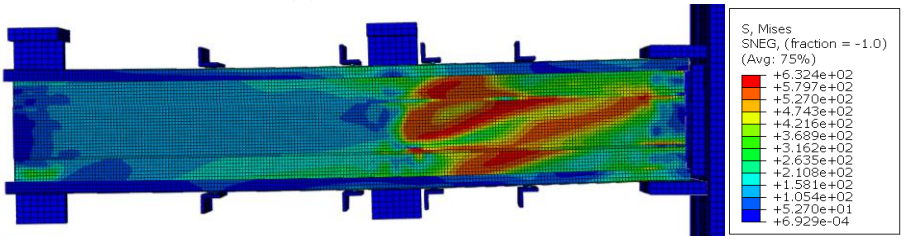

(e) Section SWC-I-80-5

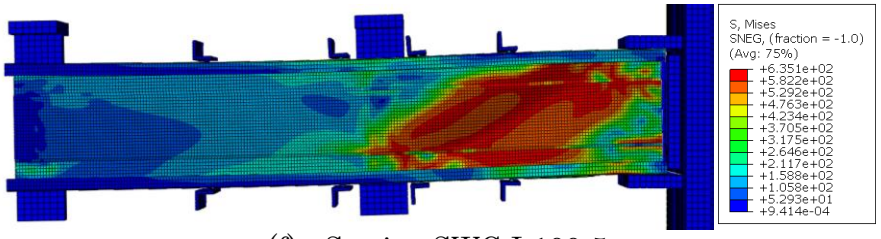

(f) Section SWC-I-100-5

Figure 3.9 Failure mode obtained from FEM simulation with an aspect ratio of 2.0

Table 3.7 ABAQUS-FEM test result summary

Section	Shear span (mm)	$V_{T,FEM}$ (kN)	$M_{T,FEM}$ (kNm)	$\frac{M_{T,FEM}}{V_{T,FEM}}$ (m)	Failure mode
C20012	400	34.78	6.66	0.19	S
SWC-I-20-5	400	39.11	7.73	0.20	S
SWC-I-40-5	400	43.07	8.84	0.21	B/S
SWC-I-60-5	400	41.71	8.44	0.20	B/S
SWC-I-80-5	400	37.75	7.18	0.19	S
SWC-I-100-5	400	36.19	6.14	0.17	S

S=mainly shear, B/S=combined bending and shear, B then S= bending then shear

Fig. 3.9 shows the shear load versus vertical displacement curves for all the FEM simulations. In general, the plotted curves show good agreement with the expected outcomes regarding the shear over displacement progress. Further, four out of the six curves reach a peak value except for two models that could not reach their full capacity, as shown in Fig. 3.8 (c) and (d). Moreover, it can be seen that every simulation has their displacement path; however, they all are grouped in two initial elastic paths. Thus the models FEM-C20012, FEM-SWC-I-80-5 and FEM-SWC-I-100-5 have the same initial path, but, at some point, they bifurcate and make their final inelastic path. Similarly, models FEM-SWC-I-20-5, FEM-SWC-I-40-5 and FEM-SWC-I-60-5 have the same initial path, but FEM-SWC-I-40-5 bifurcates before the other two.

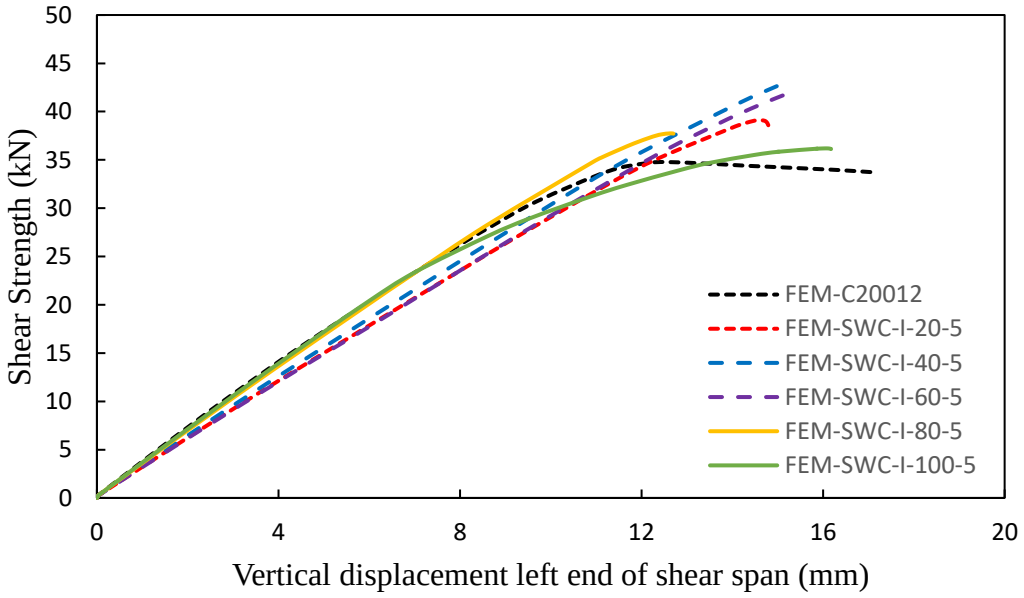

Figure 3.10 Shear strength load versus vertical displacement curves of the FEM simulations with aspect ratio 2.0

In order to determine the shear buckling of the studied sections, an eigenvalue buckling analysis was performed by using the FEM simulations built for the shear strength. Once the eigenvalues were determined, they were escalated to get the shear buckling load finally. Table 3.8 summarised the outcomes for the five stiffened web channels and unstiffened channel.

Table 3.8 ABAQUS-FEM results of shear buckling

Section	Aspect ratio	Shear span (mm)	V_{cr} (kN)
C20012	2.0	400	13.08
SWC-I-20-5	2.0	400	40.05
SWC-I-40-5	2.0	400	53.49
SWC-I-60-5	2.0	400	57.41
SWC-I-80-5	2.0	400	43.32
SWC-I-100-5	2.0	400	32.94

4. DIRECT STRENGTH METHOD FOR COLD-FORMED PURLINS WITH LONGITUDINAL STIFFENERS IN SHEAR

4.1. General

The North American Specification (AISI S100:2016) and Australian-New Zealand Standard (AS/NZS 4600:2018) for cold-formed steel (CFS) members have recently incorporated Direct Strength Method (DSM) design rules for members in pure shear. However, we will refer to the AISI S100:2016 standard for this investigation. That said, two different conditions are proposed to determine the nominal shear strength, one that excludes the Tension Field Action (TFA) and another that includes the TFA. Both DSM shear design rules have been used in the present numerical research. To be more precise, the plain-lipped channel aligns with the shear design rule with TFA, while the channels with longitudinal web stiffeners line up with the shear design rule without TFA. The DSM of shear design for CFS members is extensively detailed in section 2.3.2, but it is graphically represented in Fig 4.1, where the DSM shear design curves with and without TFA are shown. Finally, the objective of the present chapter is to compare the FEM test results against the DSM shear curves plotted in Fig. 4.1.

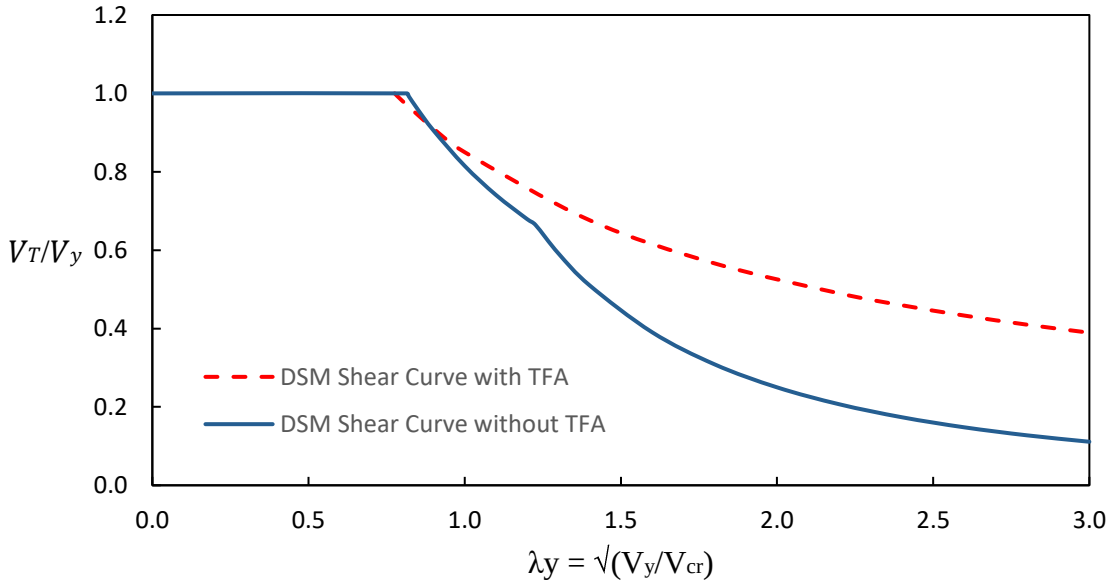

Figure 4.1 DSM shear curves

4.2. Shear yielding load V_y

In order to plot the FEM test result, three different values needs to be determined and these are the FEM shear strength ($V_{T,FEM}$), the shear buckling load (V_{cr}), and the shear yielding load (V_y).

In chapter 3, $V_{T,FEM}$ and V_{cr} have been already determined, but the V_y values are missing, and are determined based on the following equation $V_y = 0.6A_wF_y$, where A_w is the area of the web member and F_y is the design yield stress. Table 4.1 summarises the calculations to obtain V_y loads of six members under study finally. Further, the members with longitudinal web stiffeners have the same shear yielding load because the thickness, web width and the yield stress for all of them are the same.

Table 4.1 Shear yielding loads for the sections under study with aspect ratio of 2.0

Section label	t (mm)	d_w (mm)	A_w (mm^2)	F_y (MPa)	V_y(kN)
C20012	1.2	194.80	233.76	584.2	81.94
SWC-I-20-5	1.2	198.94	238.73	584.2	83.68
SWC-I-40-5	1.2	198.94	238.73	584.2	83.68
SWC-I-60-5	1.2	198.94	238.73	584.2	83.68
SWC-I-80-5	1.2	198.94	238.73	584.2	83.68
SWC-I-100-5	1.2	198.94	238.73	584.2	83.68

4.3. Comparison of Direct Strength Method (DSM) for shear design with purlins with longitudinal stiffeners and aspect ratio of 2.0

As presented in the parametric study within Chapter 3, a series of numerical simulations were performed on plain-lipped channels and stiffened web channels with an aspect ratio of 2.0 using the FEM version of the Dual Actuator Test Rig. The FEM simulations results of shear strength ($V_{T,FEM}$) and shear elastic buckling (V_{cr}) for the analysed channels are summarised in Table 4.2. Additionally, the table includes the shear yield loads (V_y), the shear slenderness ($\lambda_v = \sqrt{V_y/V_{cr}}$) and the ratio value of $V_{T,FEM}/V_y$.

Table 4.2 FEM simulation results and DSM shear design loads for sections under study

Section	Aspect ratio	$V_{T,FEM}$ (kN)	V_{cr} (kN)	V_y (kN)	$\sqrt{V_y/V_{cr}}$	$V_{T,FEM}/V_y$
C20012	2.0	34.78	13.08	81.94	2.50	0.42
SWC-I-20-5	2.0	39.11	40.05	83.68	1.45	0.47
SWC-I-40-5	2.0	43.07	53.49	83.68	1.25	0.52
SWC-I-60-5	2.0	41.71	57.41	83.68	1.21	0.50
SWC-I-80-5	2.0	37.75	43.32	83.68	1.39	0.45
SWC-I-100-5	2.0	36.19	32.94	83.68	1.59	0.43

The results on last two columns of Table 4.2, $\sqrt{V_y/V_{cr}}$ and $V_{T,FEM}/V_y$, are point coordinates to be plotted on the DSM shear curves with and without TFA, in order to verify the accuracy of the FEM simulations with the DSM design provisions. It can be seen in Fig. 4.2 that in general, the FEM test results follow the design shear curves. Thereby, the test point of plain-lipped channel (FEM-C20012) lies below and really close to the DSM shear curve with TFA. Meanwhile, the test points for stiffened web channels generally lay below the DSM shear curve without TFA, as seen in Fig. 4.2. To be more specific, FEM-SWC-I-20-5 lies really close but below, FEM-SWC-I-40-5 and FEM-SWC-I-60-5 both lay far below, FEM-SWC-I-80-5 lies below and close. Finally, FEM-SWC-I-100-5 is the only one which lies above and really close.

4.4. Agreement of FEM simulations with the DSM shear curves

In order to verify the agreement of the FEM test results with the DSM shear curves; they are plotted together, as shown in Fig 4.2. So, the FEM outcomes will be discussed each by one. Let us start for the plain-lipped section labelled as FEM-C20012, its failure mode is pure shear, and it develops a TFA throughout the channel web. Moreover, the test point plotted on the DSM shear curves almost perfectly match the curve with TFA; this fact confirms that the DSM shear curve with TFA is applicable for members with an aspect ratio of 2.0.

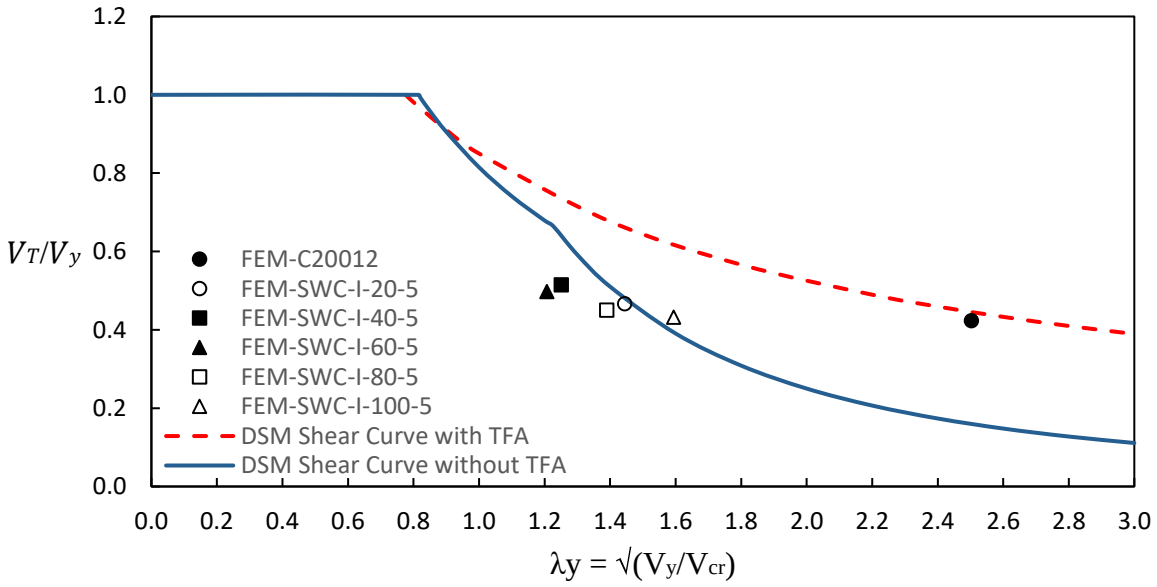

Figure 4.2 FEM simulation results with an aspect ratio of 2.0 versus DSM shear curves

Let us now analyse the channels with inclined web stiffeners and aspect ratio of 2.0, starting from the smallest to the most extended stiffener depth. For labelled section FEM-SWC-I-20-5, the longitudinal stiffener prevents TFA from developing, which increase its shear

capacity until it fails in pure shear. Besides, when the test point is plotted on the DSM curves, it lies below but really close to the DSM curve without TFA, showing good agreement with the design curve. In the case of simulations FEM-SWC-I-40-5 and FEM-SWC-I-60-5, the TFA is not developed at all; thus, the failure mode is not pure shear instead is combined with bending. Consequently, both test points lay far below the DSM shear curve without TFA and do not follow the design curve. On the other hand, for sections FEM-SWC-I-80-5 and FEM-SWC-I-100-5, the TFA is developed on the depth of longitudinal stiffeners, failling in pure shear. As a result, FEM-SWC-I-80-5 and FEM-SWC-I-100-5 lie close to the DSM shear curve without TFA and follow well the design curve; however, the first one lies below the curve while the second lies above.

5. DISCUSSIONS

5.1. General

In this Chapter, the outcomes obtained from the numerical simulations will be extensively discussed to come up with some insights about the influence of longitudinal web stiffeners on CFS channel shear behaviour.

5.2. Influence of initial imperfections on shear strength

Based on the results collected in Table 3.6, Fig. 5.1 shows the influence of initial imperfections on shear strength. It can be seen that the higher is the initial imperfection the higher is the reduction of shear strength, and that the influence of initial imperfection is different for each of the studied sections. Additionally, the influence of initial imperfections for the stiffened web sections with respect to the unstiffened web section is divided into two groups. For longitudinal web stiffeners with widths of 20, 40 and 60 mm the influence is less than for the plain-lipped section, meanwhile for dimensions of 80 and 100 mm the influence is more considerable. Hence, this fact suggests that longitudinal web stiffeners may increase or reduce the initial imperfection influence on the shear strength depending on its depth size. For the studied case, therefore; it can be concluded that for inner web depth equal or lesser than 60 mm the influence of initial imperfection on the shear strength is minor than the unstiffened channel and for dimensions equal or higher than 80 mm it is more significant.

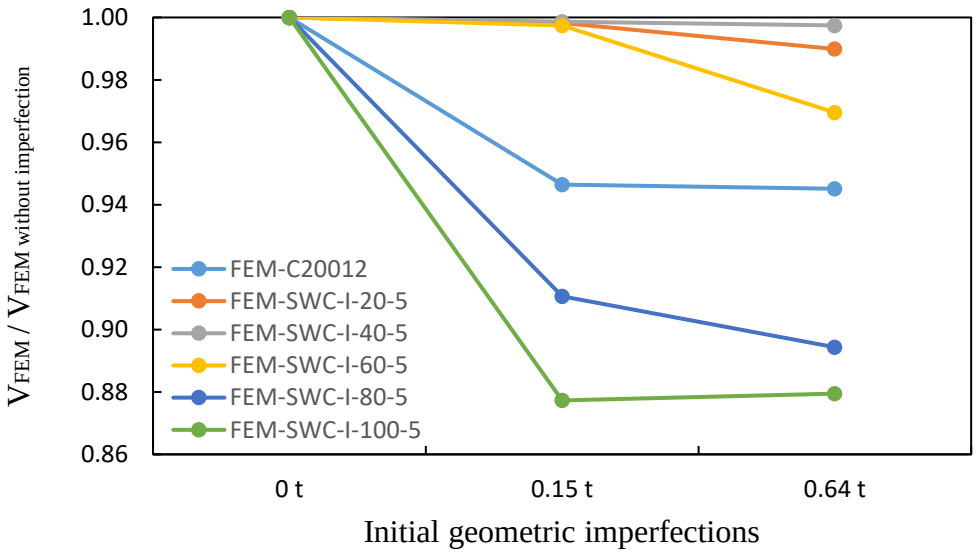

Figure 5.1 Shear strength ratio versus initial geometric imperfections

5.3. Influence of longitudinal stiffeners on failure mode

Regarding the influence of longitudinal stiffeners on the failure mode, it has been seen that for the unstiffened plain-lipped channel (FEM-C20012) the Tension Field Action (TFA) has been fully developed resulting on a pure shear failure mode. However, when longitudinal stiffeners are added to the channel web, the TFA is prevented from happening, and consequently, there is an increment on the shear stress resistance. Additionally, the TFA is developed on the inner web until it surpasses the resistance offered by the stiffener, and finally, the channel fails in pure shear as SWC-I-20-5 did. However, when the longitudinal stiffener is large enough and less stiffen, the TFA is settled on the outer web and the shear stress resistance decrease, failing again in pure shear as in channels SWC-I-100-5 and SWC-I-100-5. Nonetheless, sections SWC-I-40-5 and SWC-I-60-5 did not fail as any of the described failure modes, even though the bending moment to shear ratio was similar to the rest numerical test. A significant increment in shear capacity relative to the bending capacity may explain that fact. In such case the average moment to shear ratio of 0.2 is not enough to provoke the pure shear failure and should be reduced even more to generate pure shear failure mode.

5.4. Influence of longitudinal stiffeners on shear strength

From the results summarised in Table 3.7, it was observed that no matters what the depth of the longitudinal stiffeners is, they all improve the shear strength capacity of the channel. Furthermore, Fig. 5.2 shows the relationship between shear strength and the inner stiffener depth to channel depth ratio and a trendline was plotted for a better understanding of the plotted values.

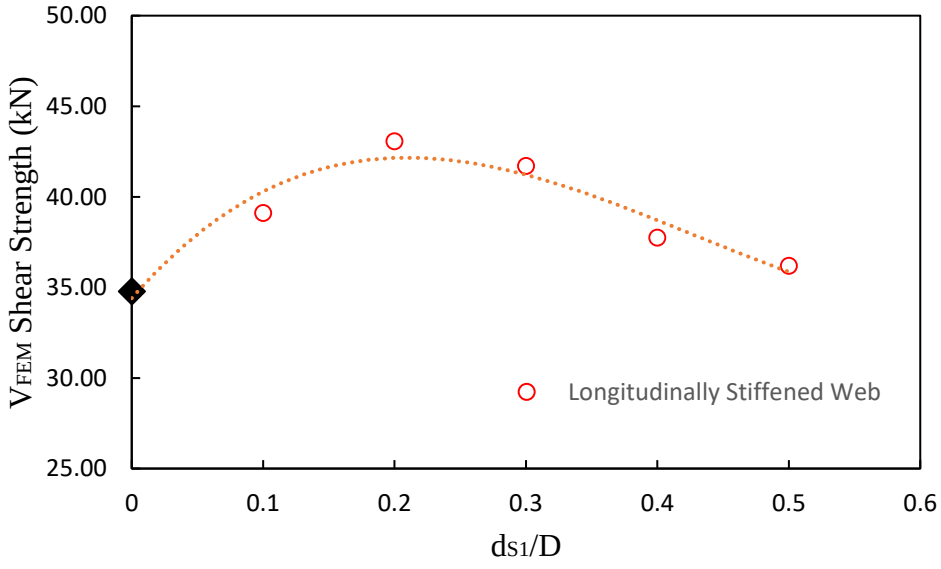

Figure 5.2 Shear strength of longitudinally stiffened web channels

It can be seen that the effectiveness of the longitudinal stiffener depends on its inner depth size. The shear strength reaches a peak value at approximate inner depth to channel depth ratio of 0.2. Further, it can be seen that the shear strength increment from 0 to 0.25 ratio is fast, while in contrast, the decrement of strength from 0.25 to 0.5 is slow. Thus, stiffened web channels with inner depth to channel depth ratio (d_{s1}/D) lesser than 0.2 are more effective to increase shear strength. Figure 5.3 shows that the longitudinal web stiffeners increase the shear strength of an unstiffened channel up to 25%, and stiffeners with d_{s1}/D ratio lesser than 0.25 are preferable.

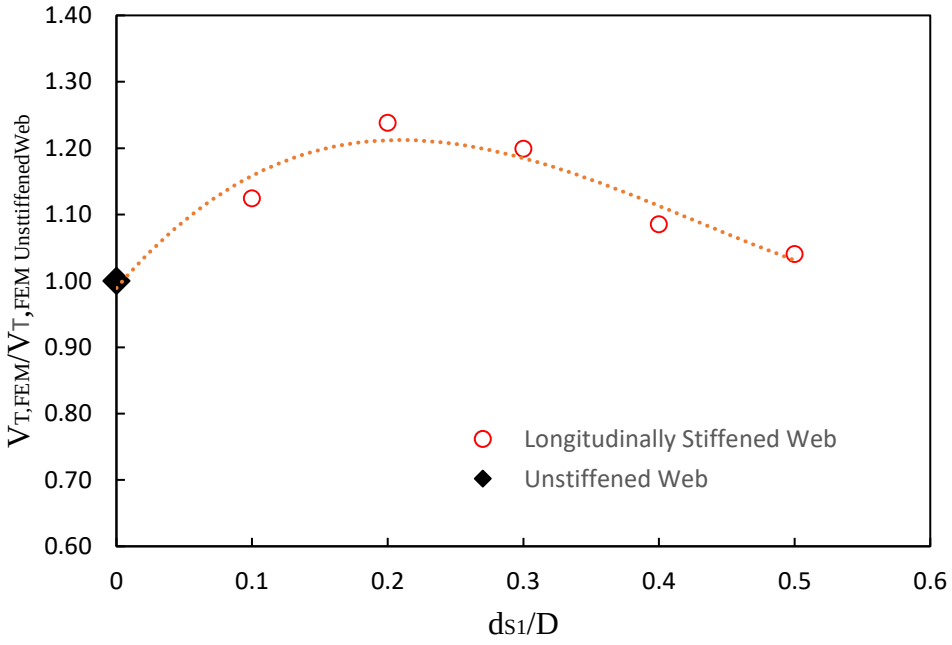

Figure 5.3 Shear strength ratio versus d_{s1}/D ratio

5.5. Influence of longitudinal stiffeners on shear buckling

As seen in Table 3.8, the addition of longitudinal stiffeners on channel web highly improves the shear buckling load for all the stiffened channels. In order to have a better insight into the influence of longitudinal stiffeners on shear buckling, the simulations results of shear buckling are plotted against the inner stiffener depth to channel depth ratio (d_{s1}/D). Fig. 5.4 shows that the shear buckling directly depends on the stiffener depth size, so the higher the stiffener depth, the greater the shear buckling. However, this relationship happens until it reaches a peak value from where an increment of depth size does not mean an increment on shear buckling anymore, oppositely, it means a decrement of shear buckling capacity as seen in Fig. 5.4. It is essential to point out that the shear strength and the shear buckling both reach a peak value at about d_{s1}/D

ratio of 0.25. Nonetheless, what tell them apart is the percentage of increment, and there is a more significant difference between them. As said before the maximum increment percentage on shear strength due to longitudinal stiffeners is about 25%, but the shear buckling can reach an increment of around 350%; thus the stiffeners have a much more considerable influence on shear buckling than on shear strength.

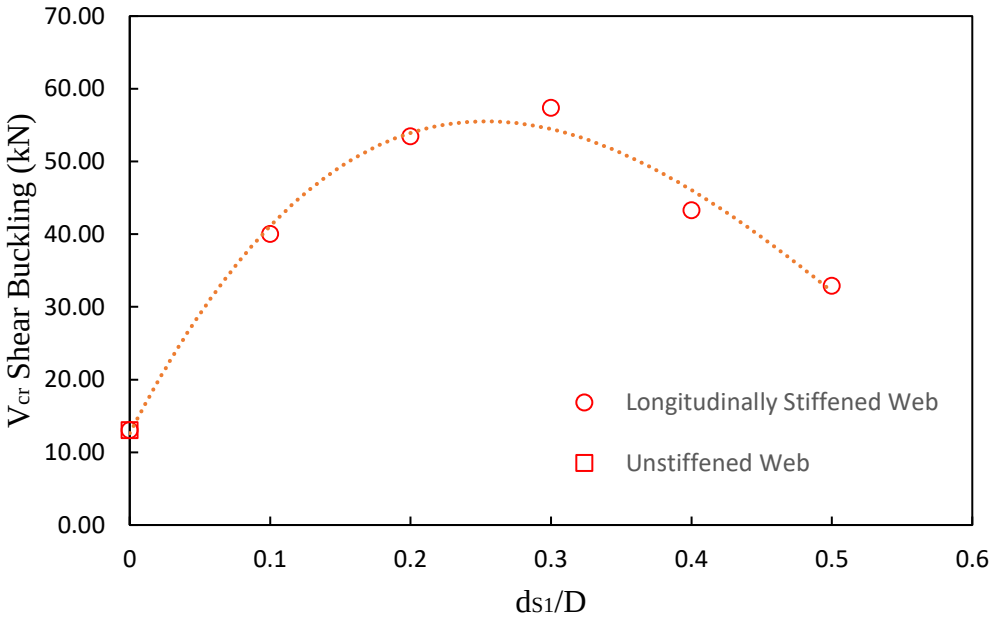

Figure 5.4 Shear buckling of longitudinally stiffened web channels

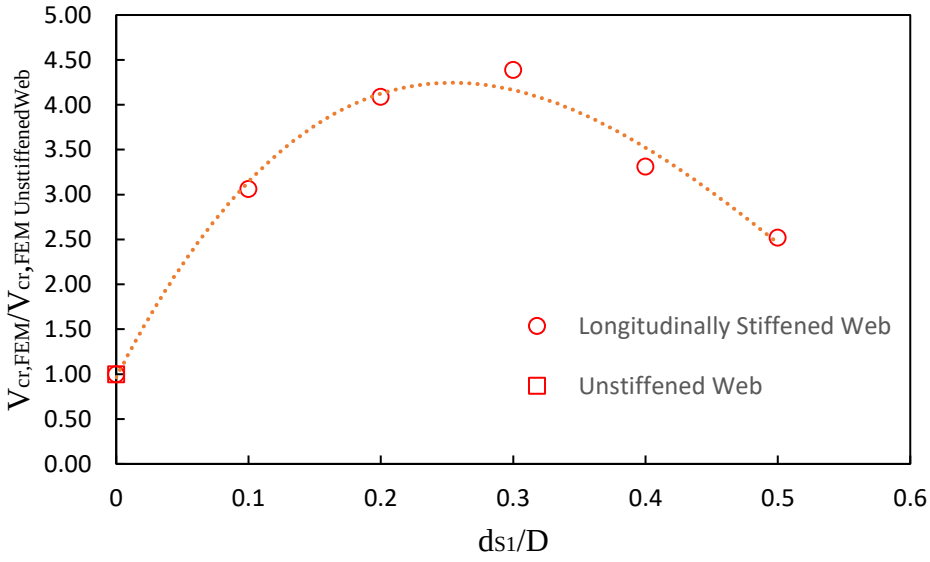

Figure 5.5 Shear buckling ratio versus d_{s1}/D ratio

6. CONCLUSIONS AND RECOMMENDATIONS

6.1. General

The research in this thesis broadens the knowledge about the shear behaviour of cold-formed steel channels, principally for members with inclined longitudinal web stiffeners and aspect ratio of 2.0. Basically, it provides a better understanding of both the shear strength and the shear buckling. Based on an experimental investigation for members with a large shear span, a numerical investigation has been conducted as part of the thesis. The FEM results have been compared with the DSM shear curves to contrast their accuracy and validate the current shear design curves.

6.2. Numerical investigations

A series of FEM-ABAQUS simulations were performed using the numerical model of the Dual Actuator Test Rig developed in The University of Sydney to study shear behaviour of members with large shear span. The specimens were purlins with longitudinally inclined web stiffeners with various depth sizes and a constant width of 5 mm. The FEM results show that for all the studied cases, the web stiffeners improve both the shear strength and buckling, but significantly more the last one. However, the effectiveness of the stiffener depends on its depth size, so the maximum shear capacity has been found when the stiffener depth to channel depth ratio d_{s1}/D is around 0.25, which mean that inclined longitudinal web stiffeners with d_{s1}/D lower than 0.25 are more effective to improve the shear capacity of the member up to 25% with respect to the unstiffened channel.

6.3. Direct Strength Method shear design

The FEM-ABAQUS results were plotted against the DSM shear curves, and in general, a good agreement was found between them, this fact suggests that the current DSM shear equations predict well the nominal shear strength for members with an aspect ratio of 2.0. Furthermore, the FEM results for channels with longitudinal web stiffeners align with the DSM shear curve without TFA, except for two FEM test results. Due to the great improvement of shear buckling, the current moment to shear ratio of around 0.20 is not enough to determine the real shear strength of the member; consequently, they do not fail in pure shear and lay far below the shear design curve. Hence, FEM results without considering these two test values follow well the DSM shear curve, proven the viability of the shear design equations with aspect ratio up to 2.0.

6.4. Recommendations for further studies

This thesis is based on numerical investigation only; therefore, experimental research must be conducted to corroborate and validate the outcomes of this investigation. Since no previous experimental studies for stiffened web channels with aspect ratio equal to or higher than 2.0 were performed before, this numerical investigation provides valuable insights for future experimental and numerical investigations. Therefore, a series of experimental tests using the Dual Actuator Test Rig should be performed to broaden the knowledge about the shear behaviour of stiffened web channels. Moreover, since this investigation only covers the study of channels with inclined web stiffeners, other types of stiffened web channels should also be researched to understand their performance better and mainly the advantages of adding longitudinal web stiffener with regards to shear strength.

REFERENCES

1. Yu, W.-w., Cold-formed steel design. 4th ed. ed, ed. R.A. LaBoube. 2010, Hoboken, N.J: Wiley.
2. Brune, B., Cold-formed steel structures. Steel Construction, 2013. **6**(2): p. 73-73.
3. Schafer, B.W., Cold-formed steel structures around the world. Steel Construction, 2011. **4**(3): p. 141-149.
4. Hancock, G.J. and C.H. Pham, New section shapes using high-strength steels in cold-formed steel structures in Australia, in Recent Trends in Cold-Formed Steel Construction. 2016, Woodhead Publishing. p. 221-239.
5. Hancock, G.J., Local, distortional and lateral buckling of I-beam. Journal of Structural Engineering, 1978.
6. Timoshenko, S., Theory of elastic stability. 2nd ed. ed. Engineering societies monographs. 1961, New York: McGraw-Hill.
7. Pham, C.H. and G.J. Hancock, Shear buckling of thin-walled channel sections. Journal of Constructional Steel Research, 2009. **65**(3): p. 578-585.
8. Hancock, G.J. and C.H. Pham, A signature curve for cold-formed channel sections in pure shear. 2011, The University of Sydney.
9. Pham, C.H. and G.J. Hancock, Shear buckling of channels using the semi-analytical and spline finite strip methods. Journal of Constructional Steel Research, 2013. **90**: p. 42-48.
10. Hancock, G.J. and C.H. Pham, Shear buckling of channel sections with simply supported ends using the Semi-Analytical Finite Strip Method. Thin-Walled Structures, 2013. **71**: p. 72-80.
11. AISI, North American Specification for the Design of Cold-Formed Steel Structural Members, S100-16th ed. 2016: Washington, D.C., U.S.A.
12. StandardsAustralia, AS/NZS 4600:2018 Cold-formed steel structures. 2018, Standards Australian/Standards New Zealand: Sydney, Australia.
13. Pham, C.H., L.A. Bruneau, and G.J. Hancock, Experimental study of longitudinally stiffened web channels subjected to combined bending and shear .(Report)(Author abstract). 2015. **141**(11).
14. Pham, C.H. and G.J. Hancock, Experimental investigation of high strength cold-formed C-sections in combined bending and shear.(Author abstract)(Report). Journal of Structural Engineering, 2010. **136**(7): p. 866.

15. Yu, W. and R. LaBoube, Webs for cold formed steel flexural members structural behavior of beam webs subjected primarily to shear stress., in Research report, University of Missouri-Rolla. 1978, University of Missouri-Rolla: Rolla, Missouri.
16. Pham, S.H., et al., Experimental validation of the Direct Strength Method for shear spans with high aspect ratios. Journal of Constructional Steel Research, 2019. **157**: p. 143-150.
17. Pham, S.H., C.H. Pham, and G.J. Hancock, Shear Buckling of Thin-walled Channel Sections with Complex Stiffened Webs, in 21st International Specialty Conference on Cold-Formed Steel Structures. 2012, Missouri University of Science and Technology: St. Louis, Missouri.
18. Pham, C.H. and G.J. Hancock, Numerical investigation of longitudinally stiffened web channels predominantly in shear. Thin-Walled Structures, 2015. **86**: p. 47-55.
19. Pham, S.H., Design of Cold-Formed Steel Beams with Holes and Transverse Stiffeners in Shear. 2018. Ph.D Thesis, The University of Sydney.